Presentation at Modis Workshop by K.N. Liou, Oct. 13, 1994

Cirrus Cloud Properties and Detection

K.N. Liou, S.C. Ou, Y. Takano, N. Rao,
P. Yang, and B. Barkey

University of Utah

- Light Scattering by Ice Crystals: Remote Sensing Implications
- Recent Development of Light Scattering by Ice Crystals
- Remote Sounding of the Optical and Microphysical Properties of Cirrus Clouds Using AVHRR Data

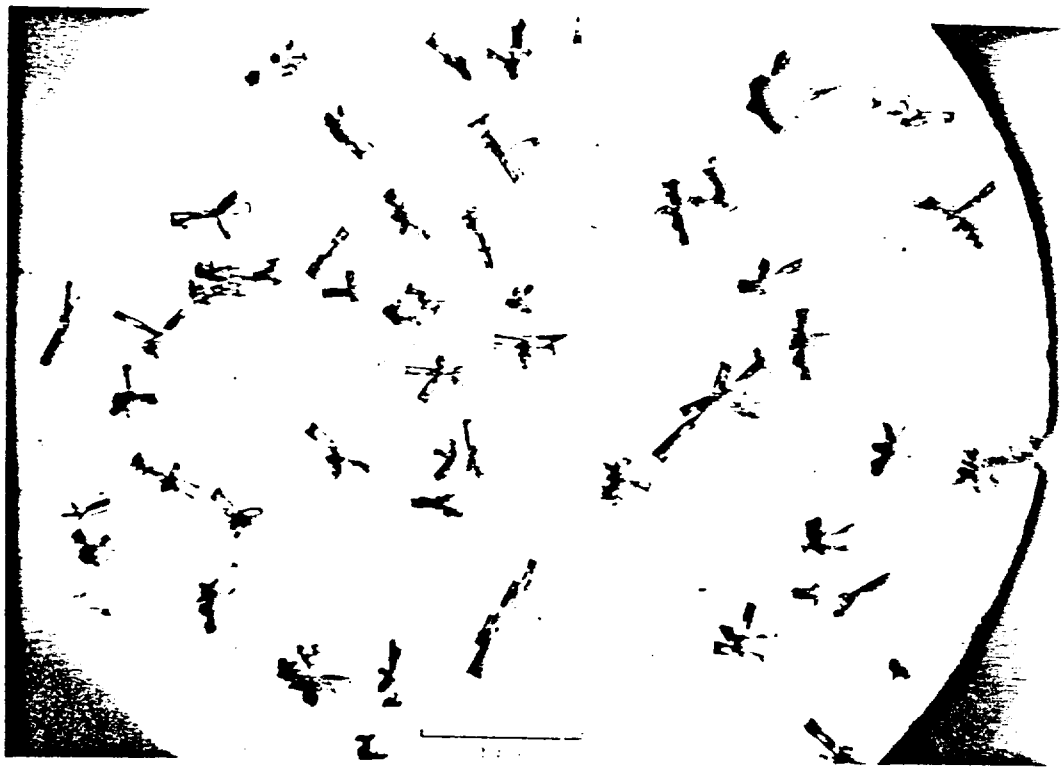

FIG. 1. Photograph of dendritic crystals [illegible]

(After Heymsfield and Knollenberg, 1972)

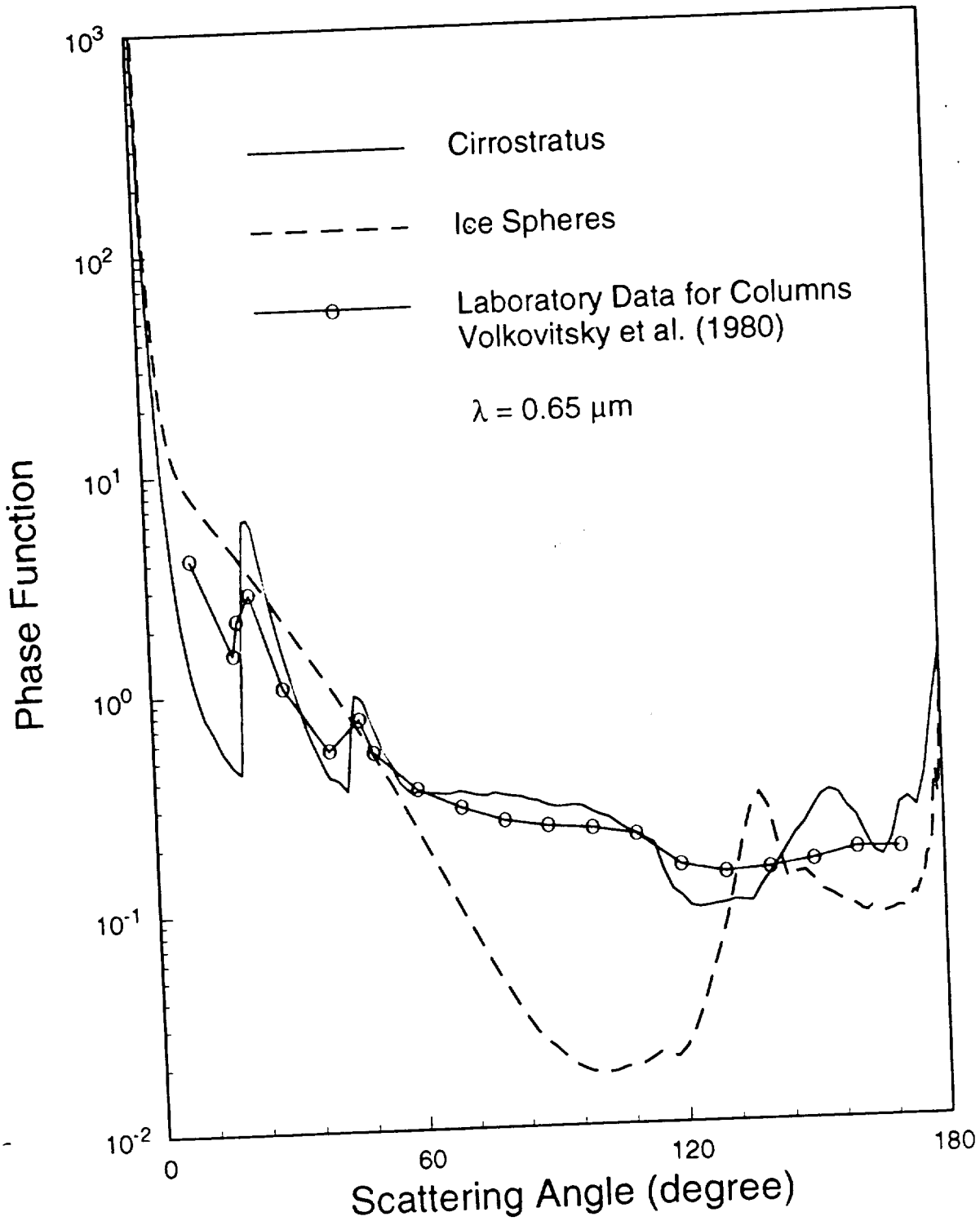
Cirrostratus
Ice Spheres
Laboratory Data for Columns
Volkovitsky et al. (1980)
λ = 0.65 μm
Phase Function
Scattering Angle (degree)
10^3
10^2
10^1
10^0
10^-1
10^-2
0
60
120
180

Satellite Remote Sensing

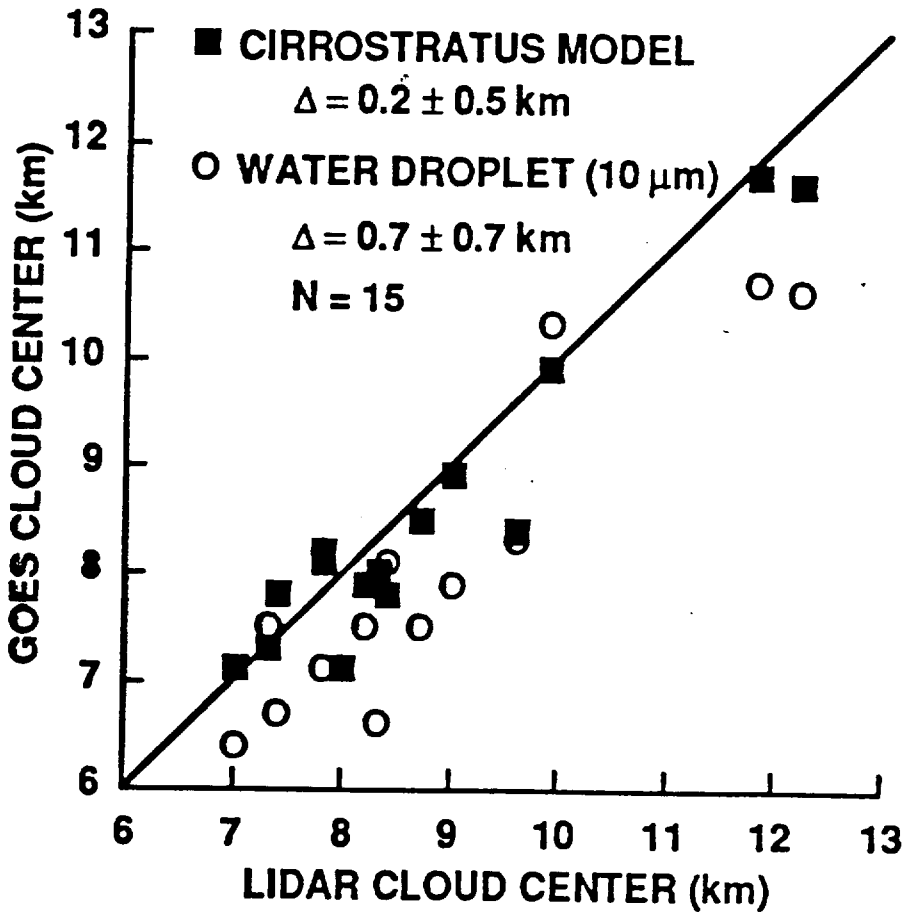

Fig. 2. Comparison of surface lidar and satellite-derived cloud-center heights over Parsons, KS. (After Minnis et al, 1992)

Spectral Radiance Data

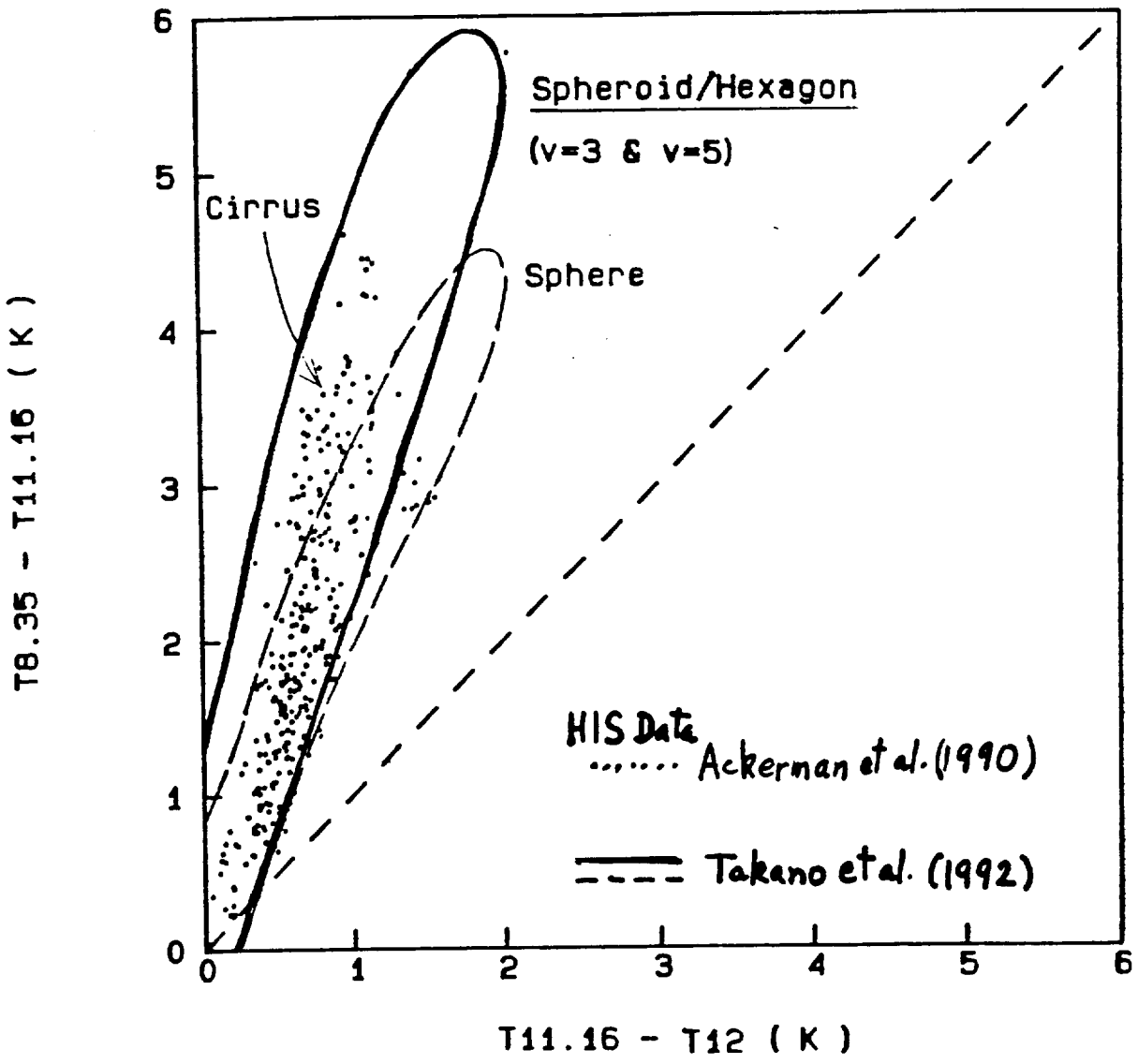

Polarization Measurement

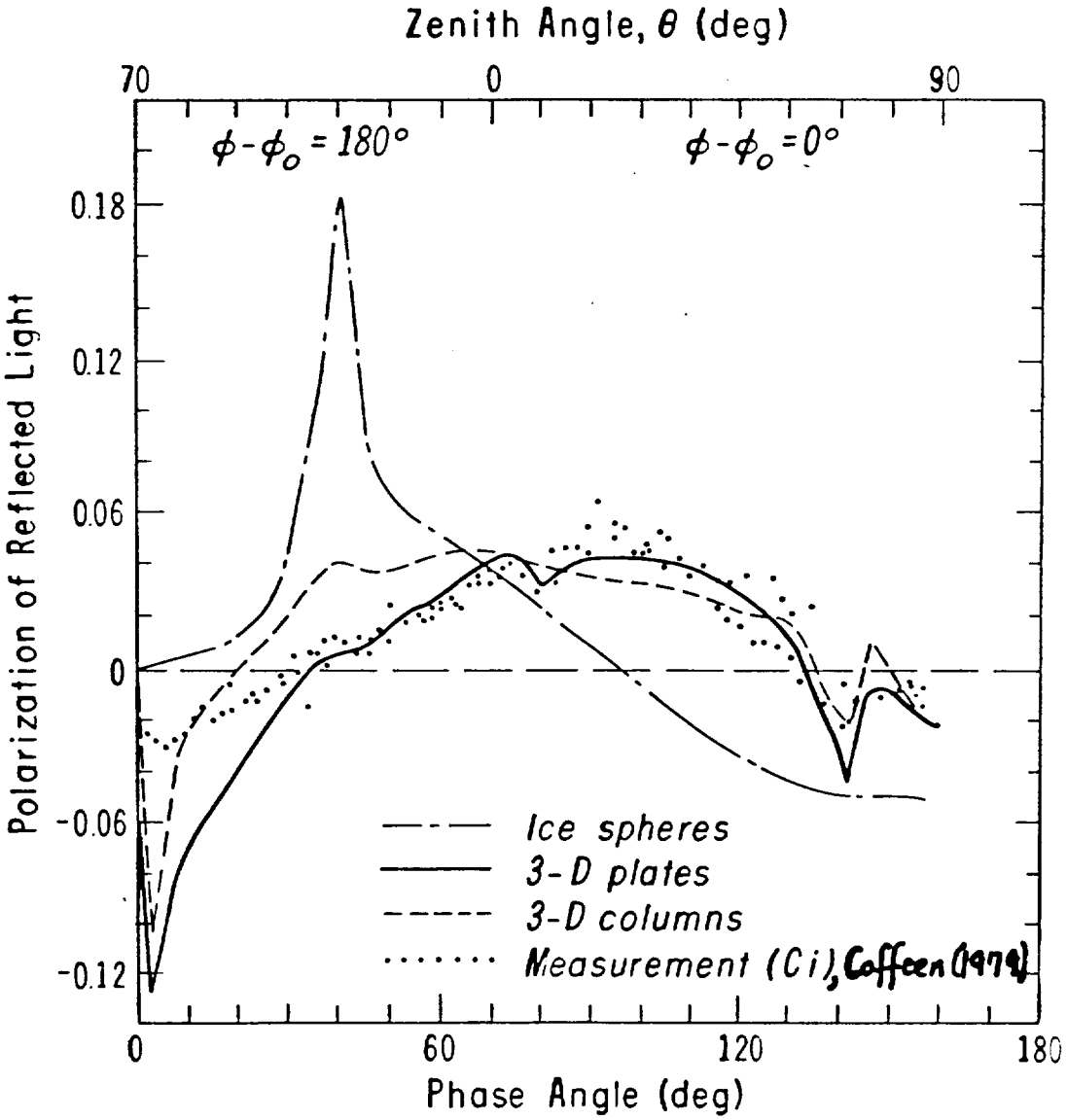

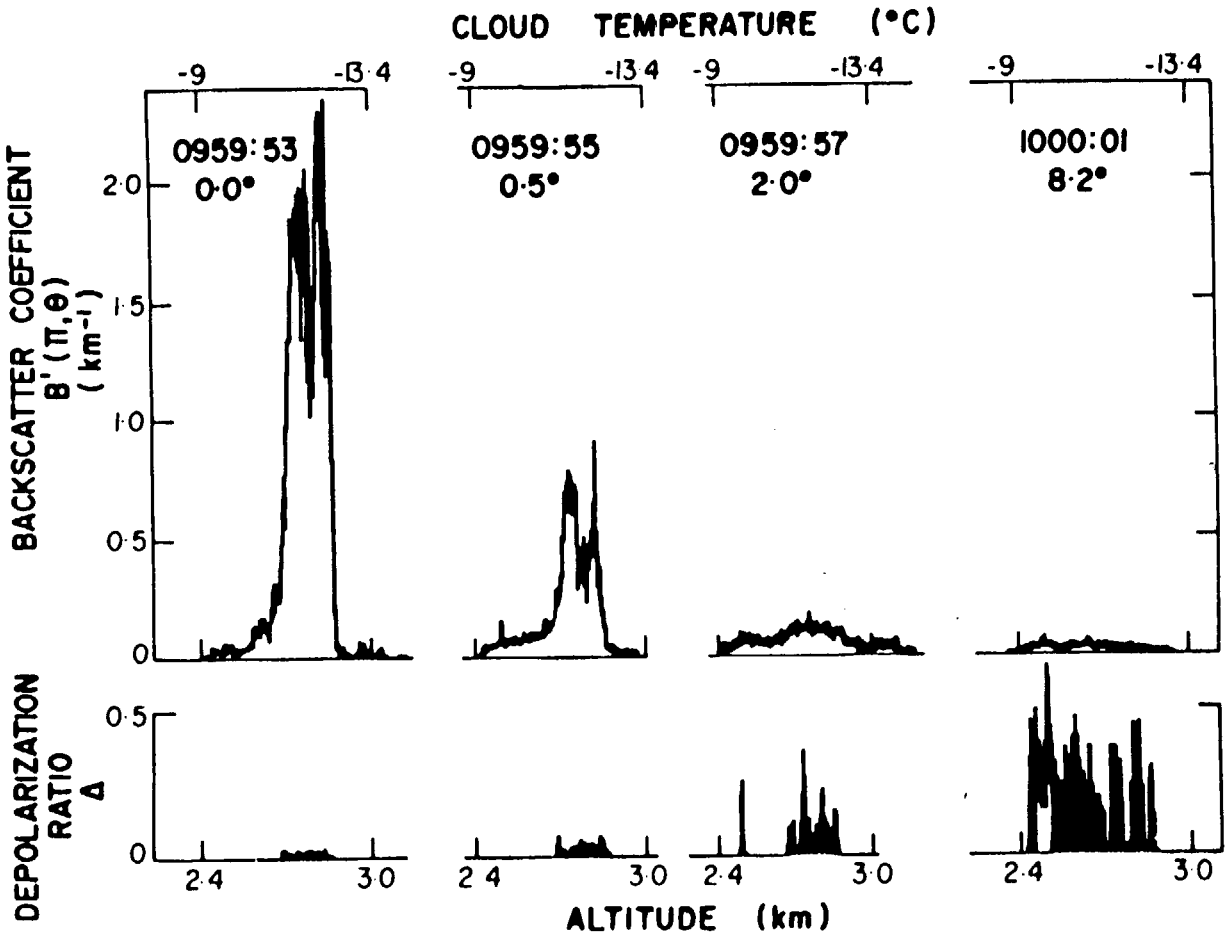

Fig. 4. Lidar field data (from Platt et al. 1978) showing the considerable decrease in planar crystal backscattering (in terms of the backscatter coefficient β') and increase in linear depolarization (Δ used here) as the lidar is scanned off the vertical direction (note the inserted times and lidar angles from the vertical direction). The cloud temperatures are within the expected range for plate crystals, and an aerial sighting of a subsun confirmed their uniform horizontal orientations.

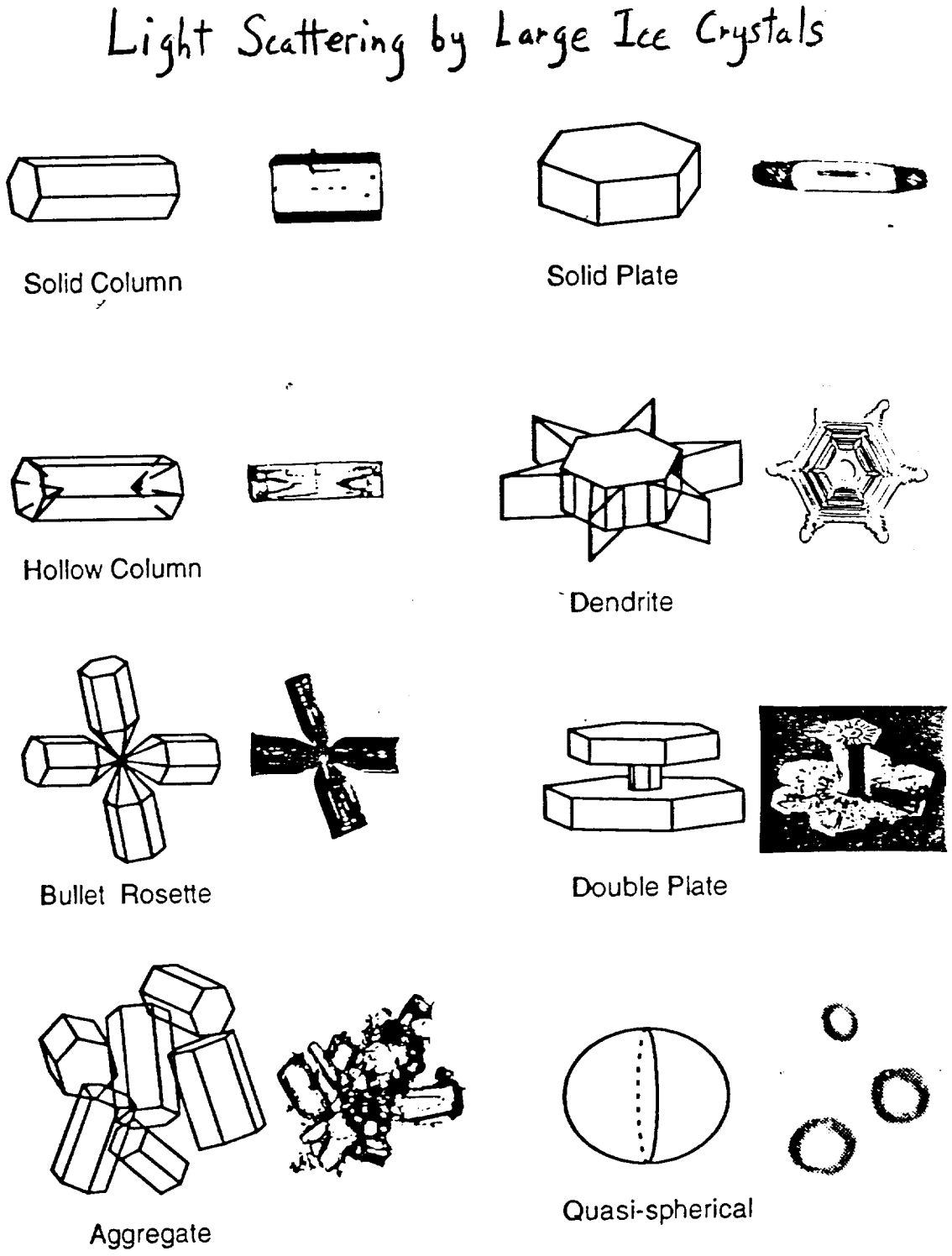

Fig. 2. The second and fourth columns depict the ice crystal shape observed in cirrus clouds. The first and third columns represent the shape simulated from a geometric model. Our current capability of solving light scattering and absorption of ice crystals includes all the shapes, except the aggregate (see text for further discussion).

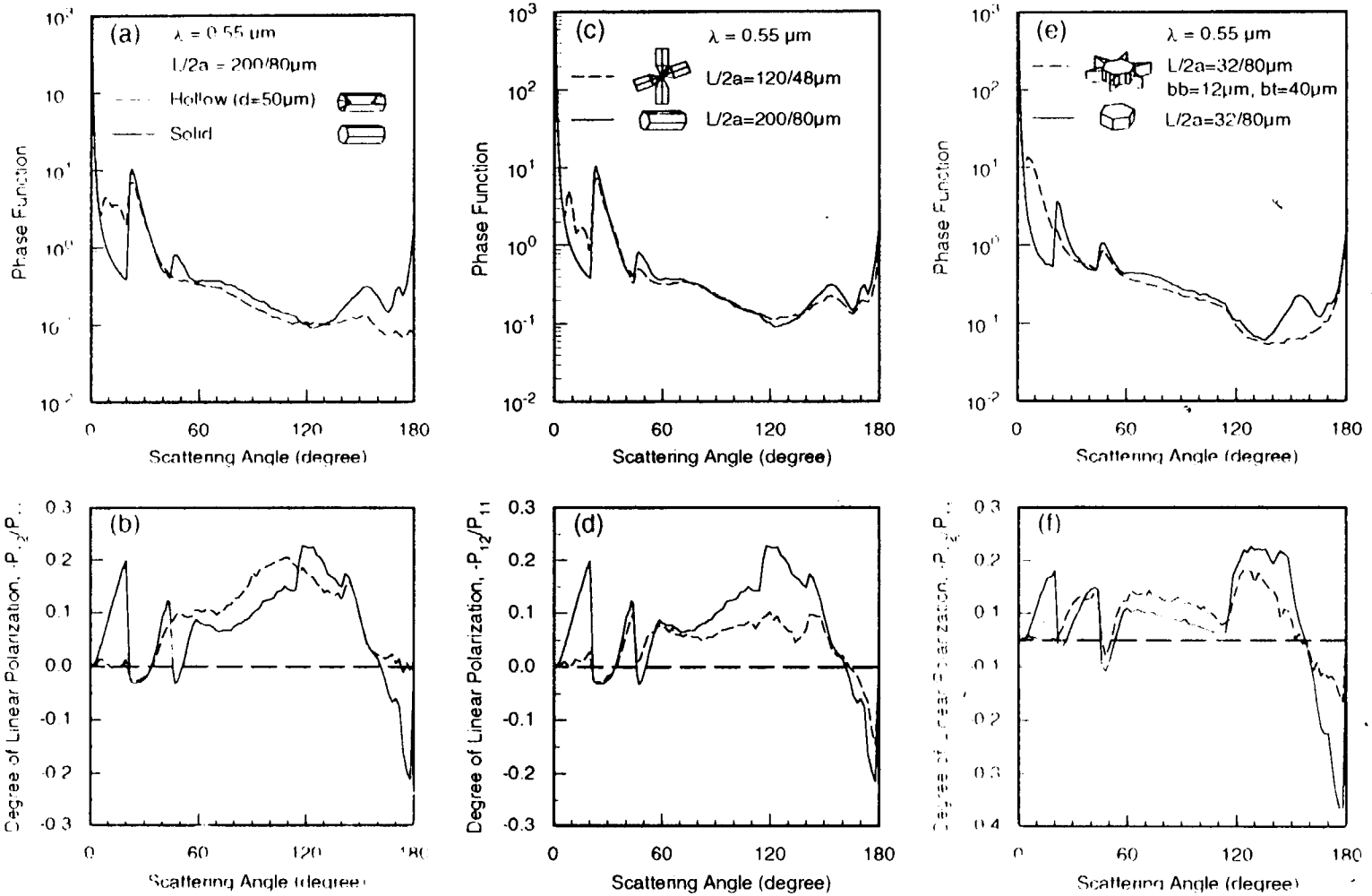

Fig.1 Phase function and degree of linear polarization as functions of the scattering angle for hollow columns (a and b), bullet rosettes (c and d), and dendrites (e and f). The wavelength and the sizes of these ice crystals are depicted in the figure, where d is the hollow depth and bt and bb are the height and width (along the side of the plate surface) of the branches of a dendrite.

FIRE II (Replica)

#28-1

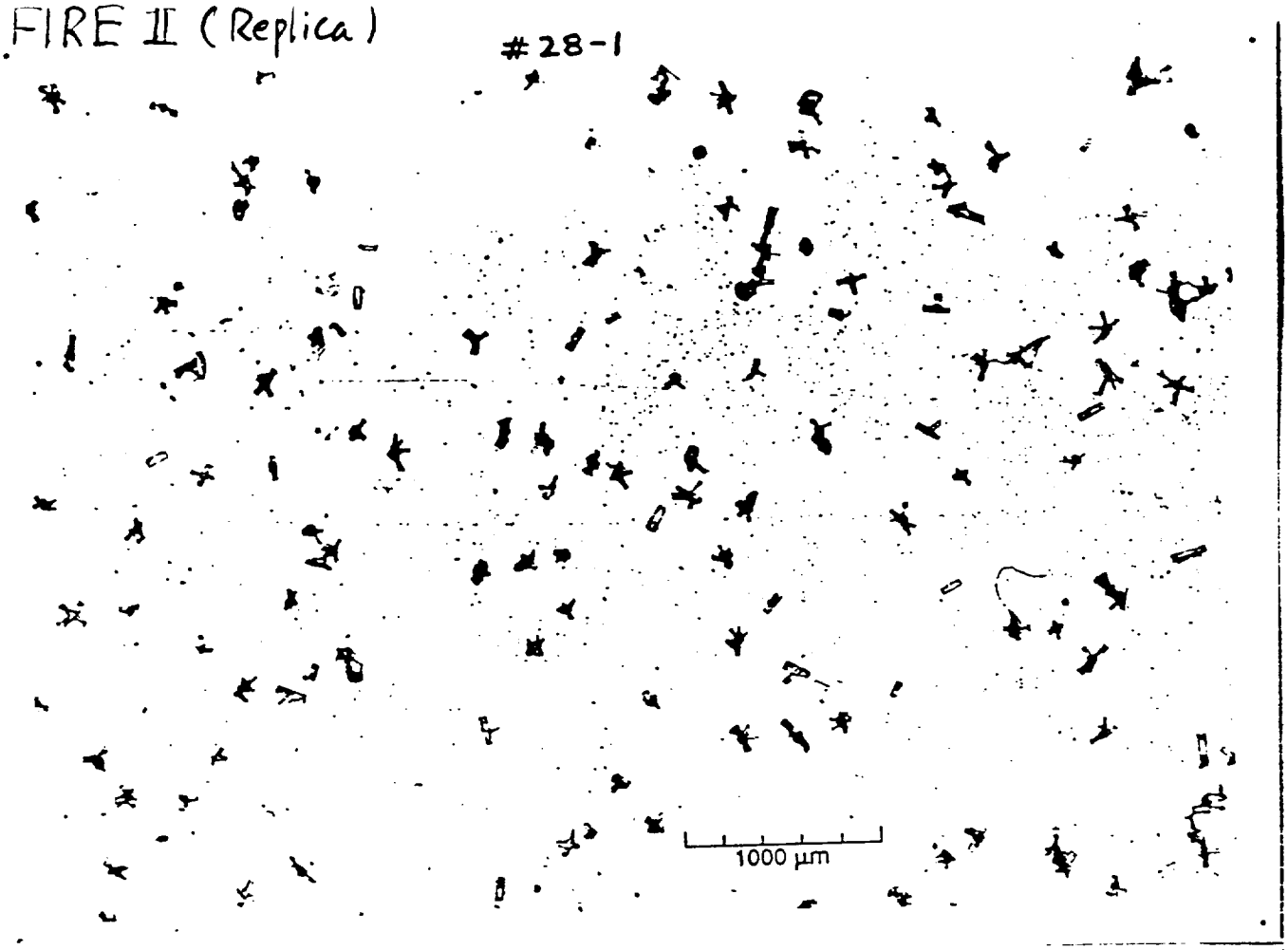

#28-2

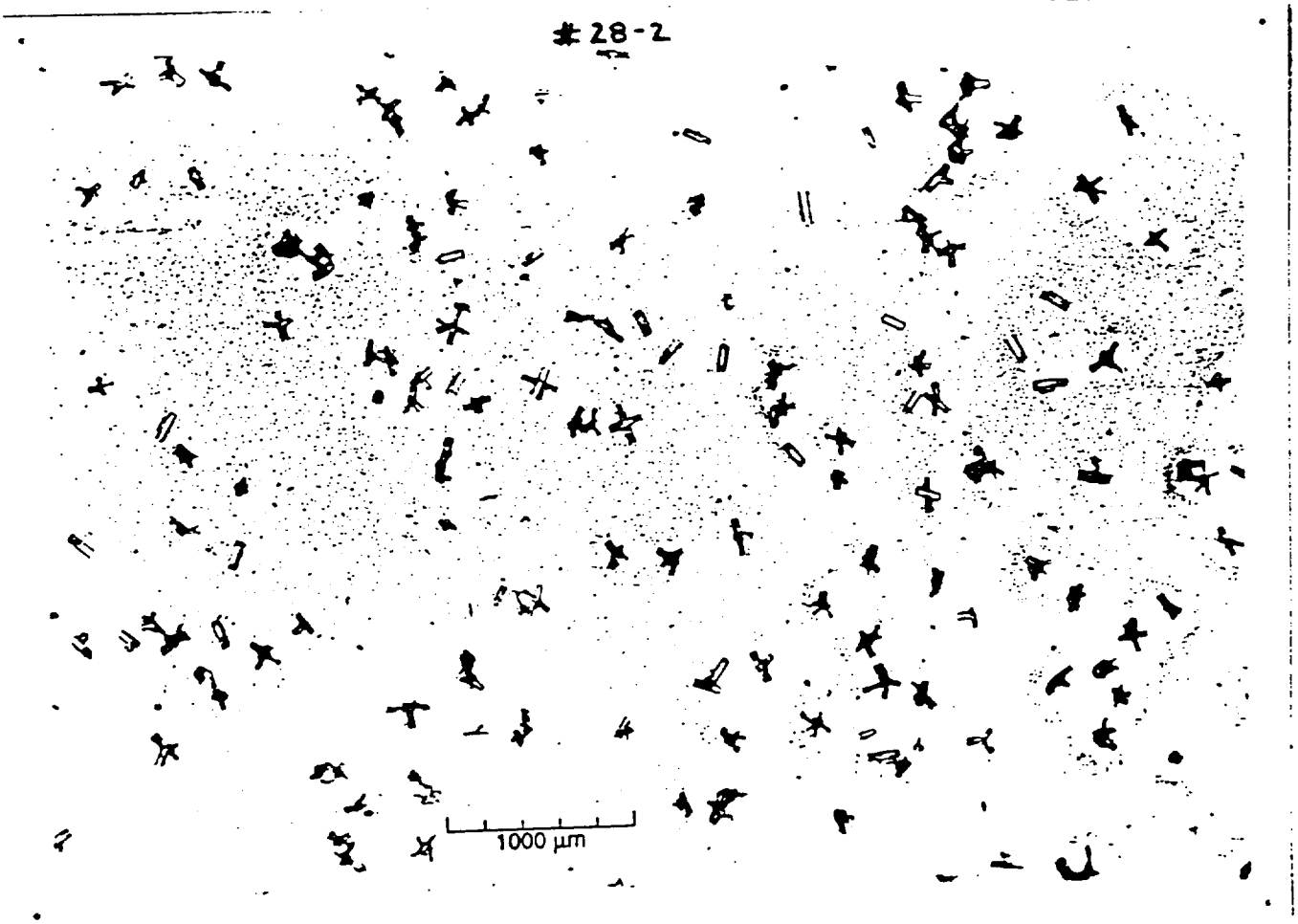

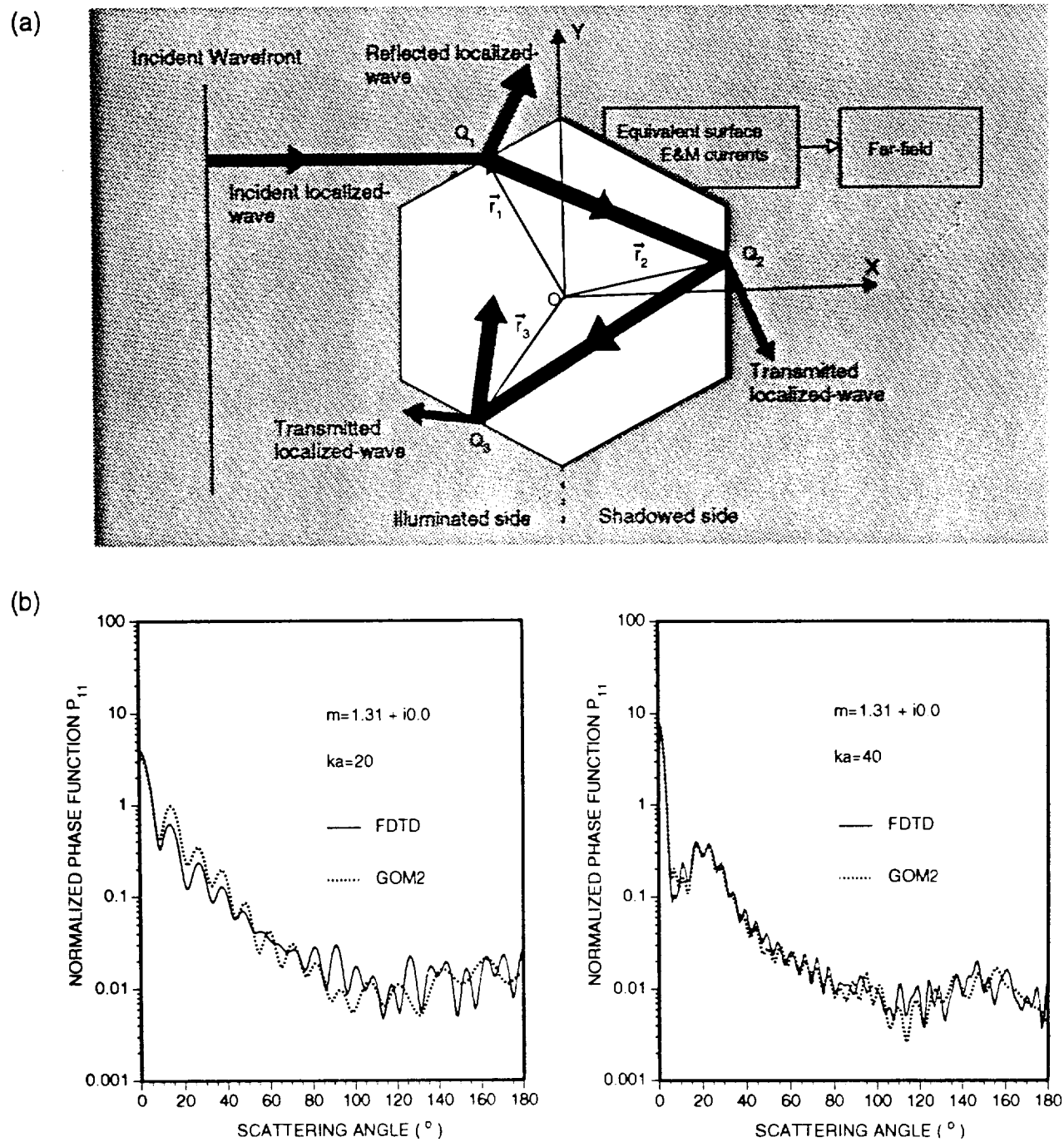

Fig. 3. (a). The conceptual diagram for the scattering of waves by a small hexagon using the geometric ray-tracing for the computation of the near field. The far field results are determined exactly by means of the electromagnetic wave theory. (b). Comparison of the phase functions for 2-D hexagonal ice columns computed from the finite difference time domain (FDTD) and the new geometric optics model (GOM2) for the size parameters of 20 and 40. Results from the time consuming FDTD are considered to be exact (Yang and Liou. 1994).

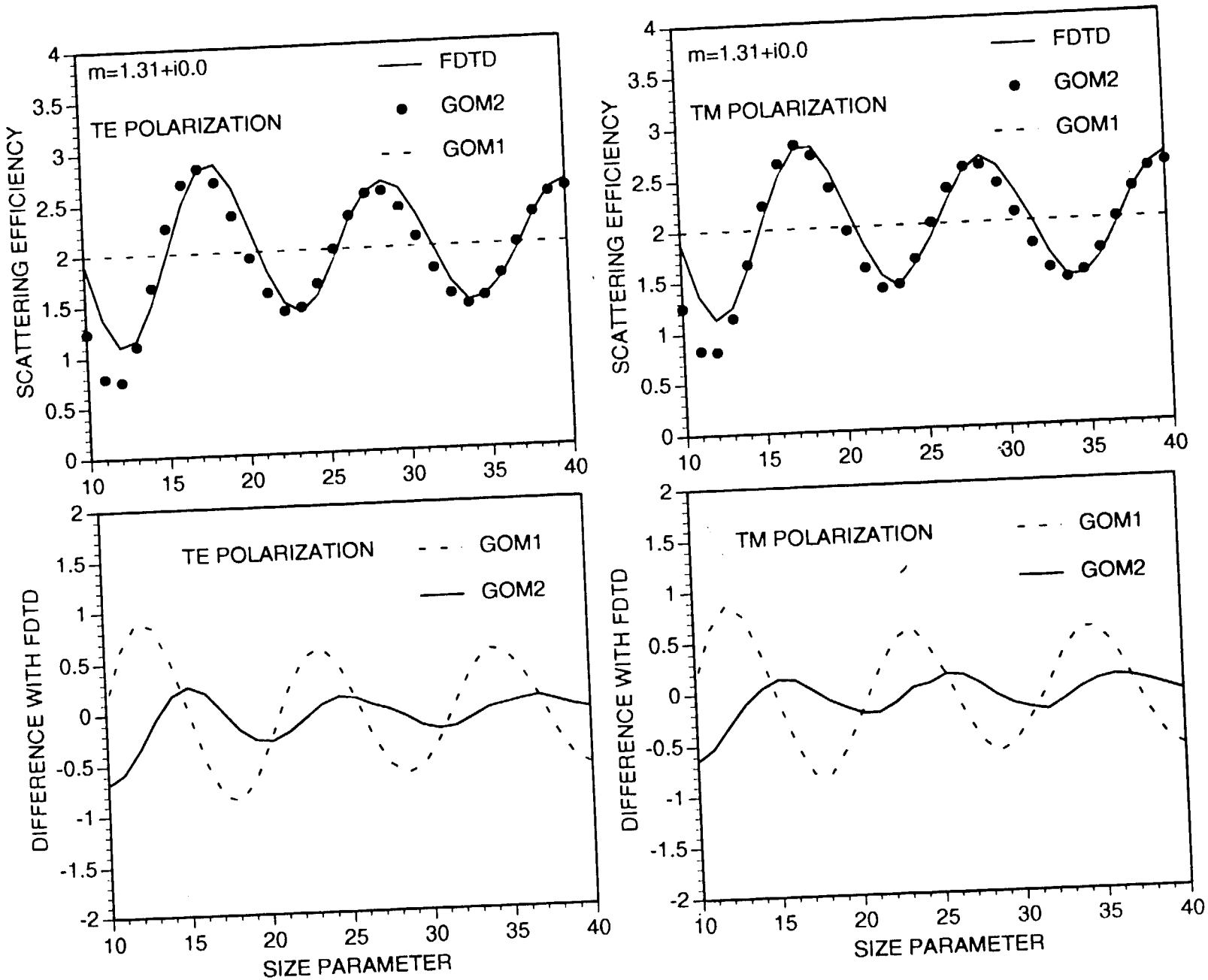
m=1.31+i0.0
TE POLARIZATION
FDTD
GOM2
GOM1
SCATTERING EFFICIENCY
m=1.31+i0.0
TM POLARIZATION
FDTD
GOM2
GOM1
SCATTERING EFFICIENCY
TE POLARIZATION
GOM1
GOM2
DIFFERENCE WITH FDTD
SIZE PARAMETER
TM POLARIZATION
GOM1
GOM2
DIFFERENCE WITH FDTD
SIZE PARAMETER

REMOTE SENSING OF CIRRUS CLOUDS: SCIENTIFIC OBJECTIVES

- Development of a retrieval scheme for the inference of cirrus cloud parameters, including mean effective ice crystal size and visible optical depth based on the principle of radiative transfer and parameterizations using the scattering and absorption properties of hexagonal ice crystals and AVHRR data, in particular, the 3.7 and 10.9 μm channel radiances. (Ou et al., Applied Optics, April, 1993)

- Removal of solar radiance in the 3.7 μm channel data for application to daytime cloud retrieval based on the correlation between the 0.63 and 3.7 μm channel radiances. (Rao et al., J. Appl. Meteor., November, 1994)

- Verification of the retrieved cirrus cloud parameters using available balloon-borne replicator and sounding observations (FIRE-II-IFO).

- Application of retrieved cirrus cloud parameters to the computation of surface radiative fluxes using a detailed radiative transfer model (Fu and Liou, 1992, 1993), and comparison with ground-based radiometer measurements.

Algorithm Development(AVHRR Chs. 3 and 4)

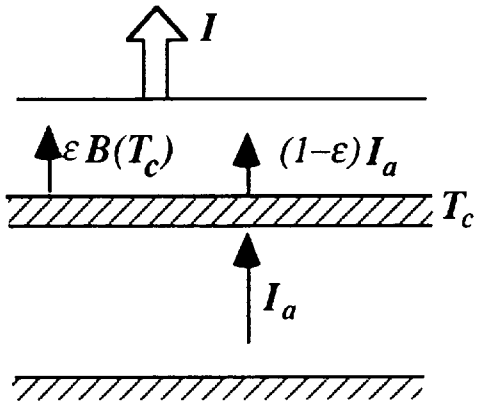

- Upwelling observed radiances

$$I_3 \cong I_{a3}(1-\varepsilon_3)+\varepsilon_3 B_3(T_c)$$
$$I_4 \cong I_{a4}(1-\varepsilon_4)+\varepsilon_4 B_4(T_c)$$

$\varepsilon_{3,4}$ = cirrus cloud IR emissivities
$B_{3,4}$ = Planck intensities
$I_{a3,4}$ = upwelling cloud-base radiances

(1) Correlation between B_3 and B_4

$$B_4(T_c)=\sum_{n=0}^{3} a_n\left[B_3(T_c)\right]^n$$

(2) Parameterization of IR emissivities

$$\varepsilon_{3,4}=1-\exp(-k_{3,4}\tau),$$

τ = visible optical depth

$$\varepsilon_4=1-(1-\varepsilon_3)^{k_4/k_3},$$

k_4/k_3 = effective extinction ratio

(3) Evaluation of $I_{a3,4}$ from three-dimensional display of the frequency of occurrence of the AVHRR radiance pair(I_3,I_4)

- Solution equation for cloud temperature

$$\left[\frac{I_3 - B_3(T_c)}{I_{a3} - B_3(T_c)}\right]^{k_4/k_3} = \left[\frac{I_4 - B_4(T_c)}{I_{a4} - B_4(T_c)}\right]$$

- Ice crystal mean effective size is defined by

$$D_e = \int_{L_{\min}}^{L_{\max}} D \bullet LDn(L)dL \Big/ \int_{L_{\min}}^{L_{\max}} LDn(L)dL$$

D = ice crystal width, L = maximum dimension

- Based on radiative transfer calculations, k_4/k_3 is parameterized in terms of $1/D_e$ as follows:

$$k_4 / k_3 = \sum_{n=0}^{2} b_n (1/D_e)^n$$

- From cloud microphysics measurements and the retrieved optical depth:

$$\overline{D_e} = \sum_{n=0}^{2} c_n (T_c - 273)^n$$

$$D_e = \{\tau / [\Delta z(\alpha + \beta / D_e)\overline{IWC}]\}^{1/3} \overline{D_e}$$

- Retrieve T_c and ε from Chs. 3 and 4 radiances and determine D_e and τ from parameterization equations

ALGORITHM DEVELOPMENT (Continued)

- Ice crystal mean effective size is defined by

$$D_e = \int_{L_{\min}}^{L_{\max}} D \bullet LDn(L)dL \Big/ \int_{L_{\min}}^{L_{\max}} LDn(L)dL$$

D = ice crystal width, L = maximum dimension

- Based on radiative transfer calculations, k_4/k_3 is parameterized in terms of $1/D_e$ as follows:

$$k_4 / k_3 = \sum_{n=0}^{2} b_n (1/D_e)^n$$

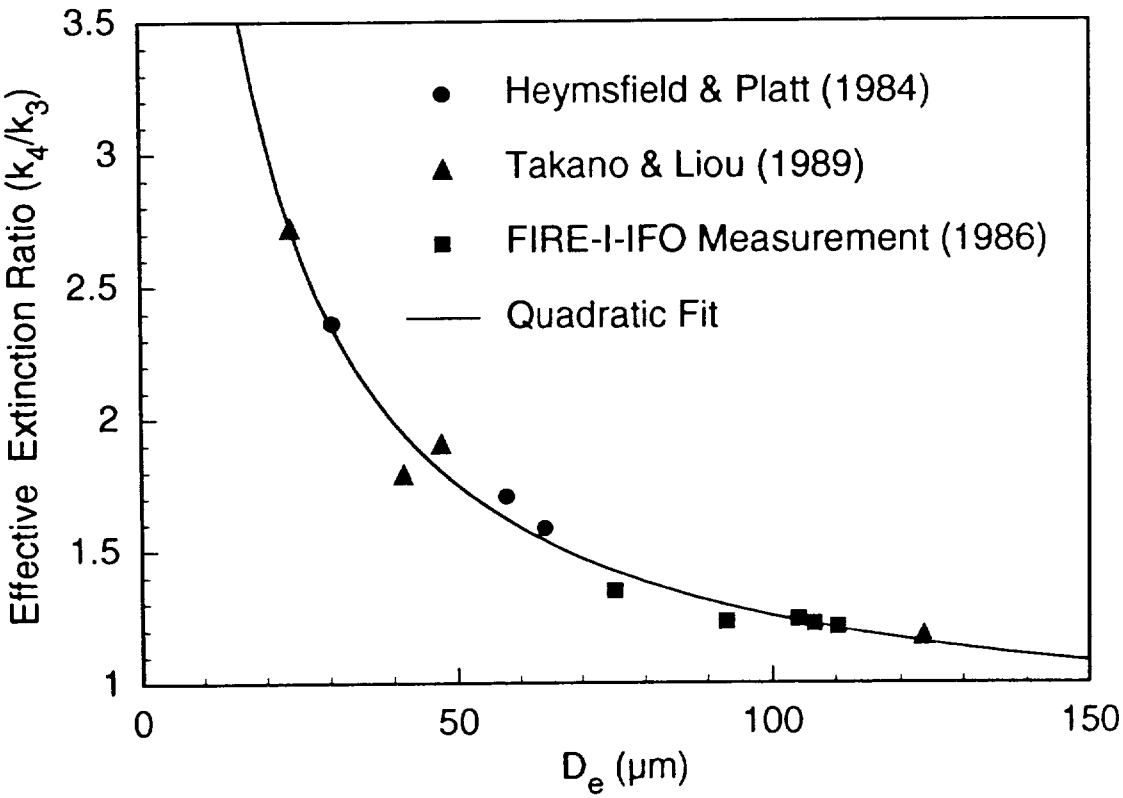

REMOVAL OF SOLAR COMPONENT IN THE 3.7 μm RADIANCE

- **Solar Reflectances for Chs. 1 (0.63 μm) and 3 (3.7μm)**

$$r_i(\mu_0,\mu,\Delta\phi) = r_i^*(\mu_0,\mu,\Delta\phi) + \frac{\gamma_i(\mu_0) r_{ai} \gamma_i(\mu)}{1 - r_{ai}\bar{r}_i(\mu,\Delta\phi)}, \quad i = 1,3$$

- **Construction of a Look-up Table Relating r_1 and r_3**

  Radiative transfer program (Takano and Liou, 1989)
  Sun-satellite geometry
  Mean effective ice crystal size

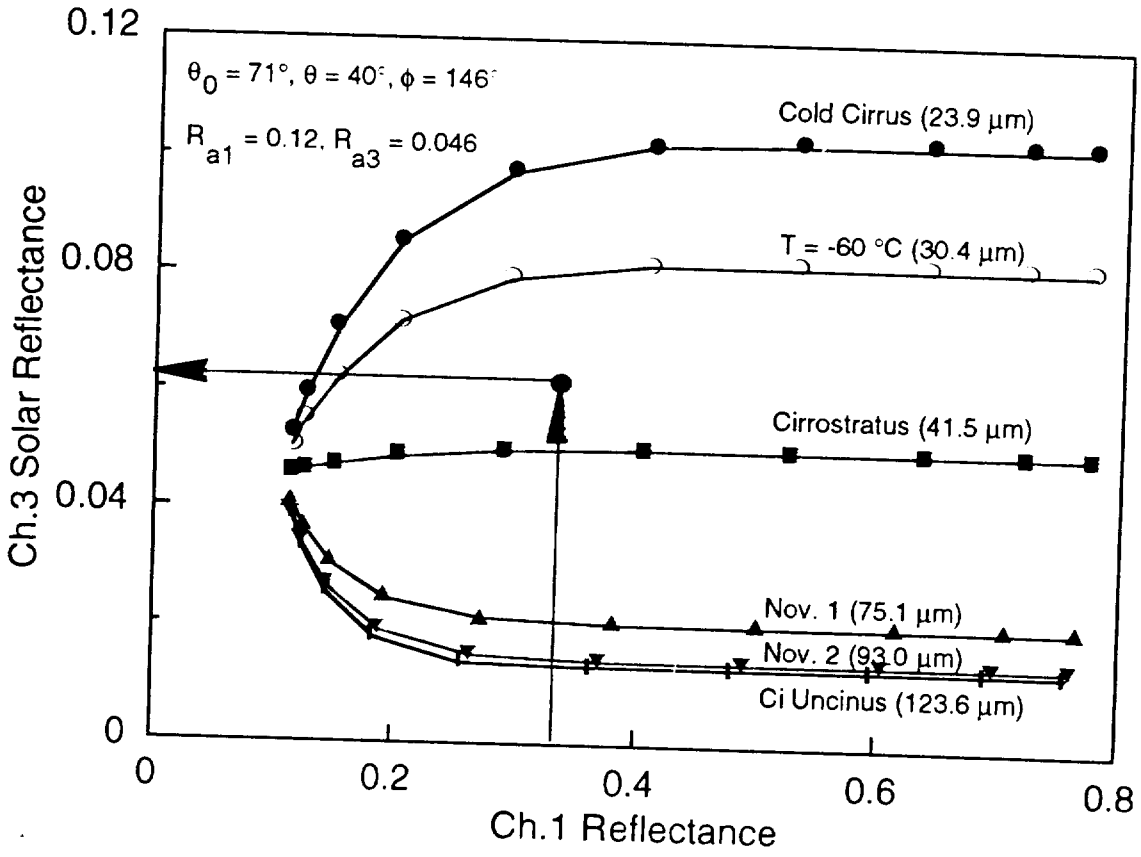

Verification (FIRE I IFO)

(a). Mean values of the retrieved T_c, ε_3, ε_4, τ, k_4/k_3, D_e, and z_c for cirrus pixels within a 1°x1° scene west of Fort McCoy at 0930 UTC, 28 October 1986, along with observed values.

Parameter	Observation	Retrieval
T_c (K)	---	244 (233-255)
ε_3	---	0.36 (0.17-0.70)
ε_4	---	0.42 (0.20-0.76)
τ	---	1.08 (0.41-2.77)
k_4/k_3	---	1.25 (1.07-1.44)
D_e (μm)	107 (King Air)	104 (68-156)
z_c (km)	6-8 (Lidar)	7.5* (6-9)

* based on the Fort McCoy sounding at 0930 UTC.

(b). Cirrus cloud temperature, cloud height, and optical depth determined from the present retrieval program.

	T_c(K)		z_c(km)		τ	
Location	present	lidar*	present	lidar*	present	GOES*
Wausau	226.5	230.7	9.5	9.0	1.54	1.43
Fort McCoy	229.7	226.5	9.1	9.5	1.5	1.41
Madison	225.6	228.1	9.6	9.3	0.6	0.56

*from Minnis et al. (1990) using lidar and GOES data at 2100 UTC, October 28, 1986

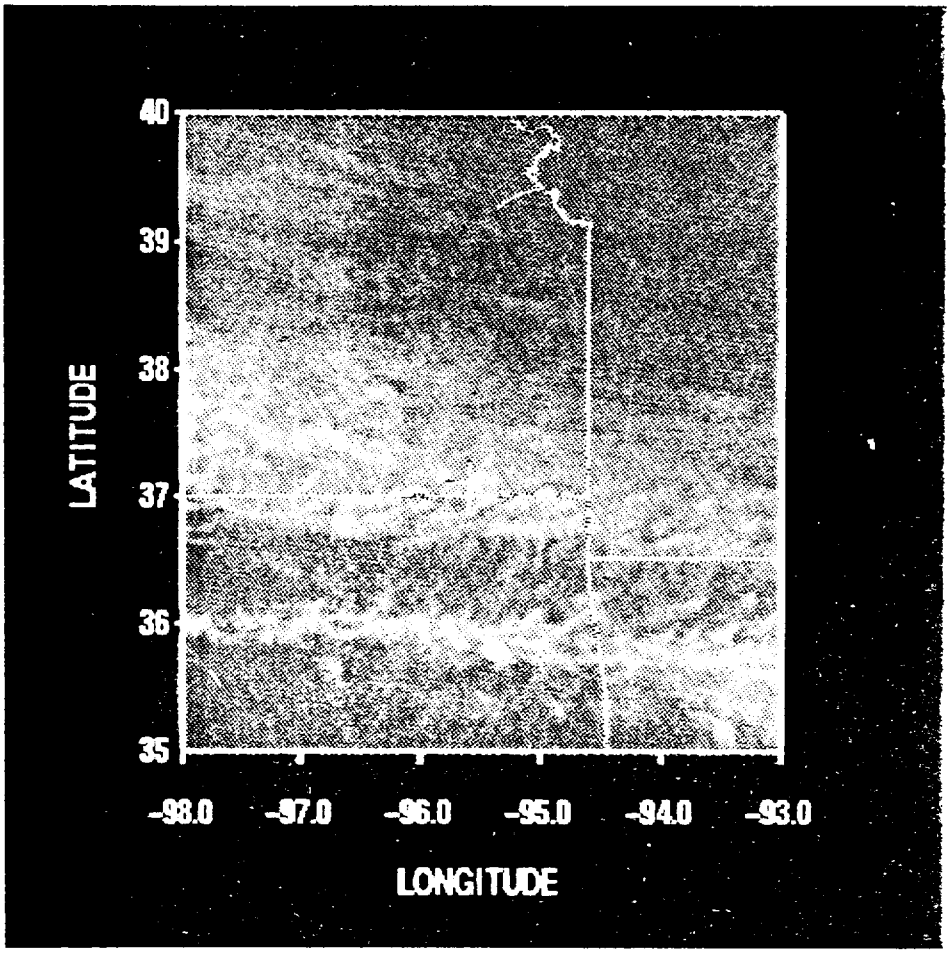

Attenuated Scattering Ratios : 12-05-91
NASA Langley Research Center 8" Lidar

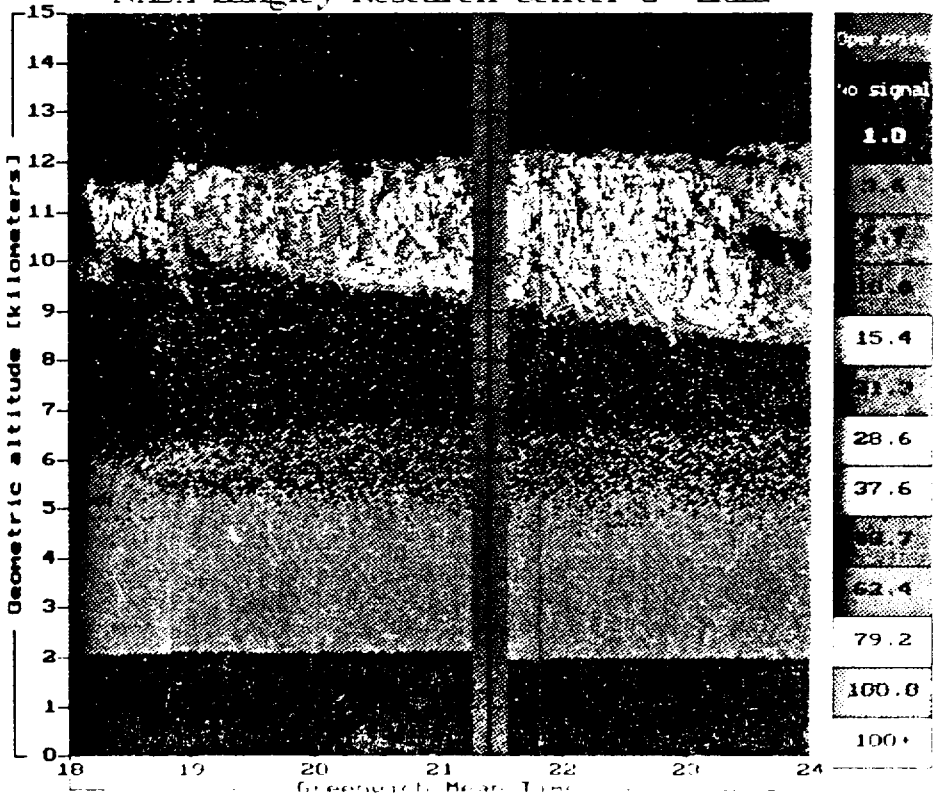

Satellite Data and Retrieval Results at
2108 UTC, 5 December, 1991

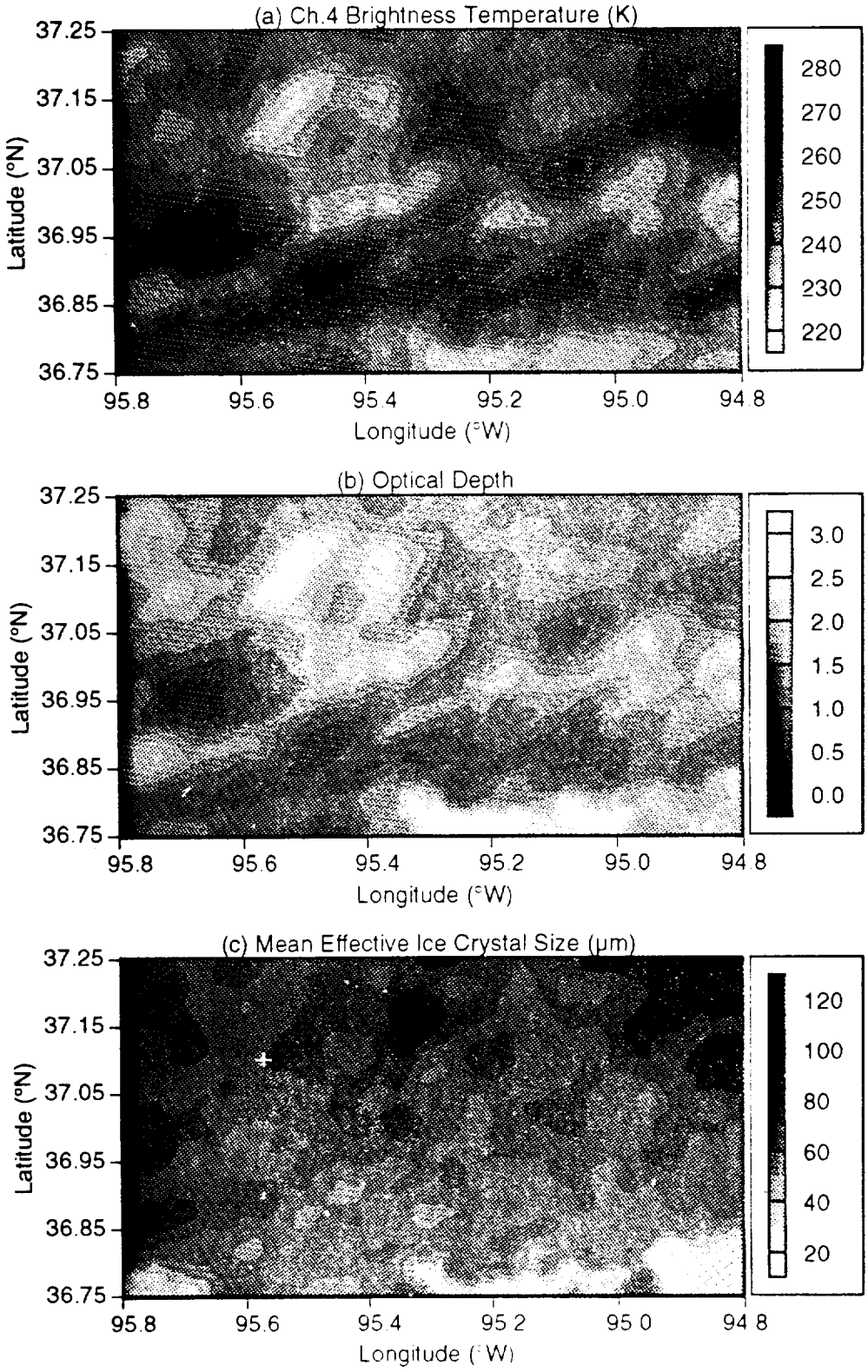

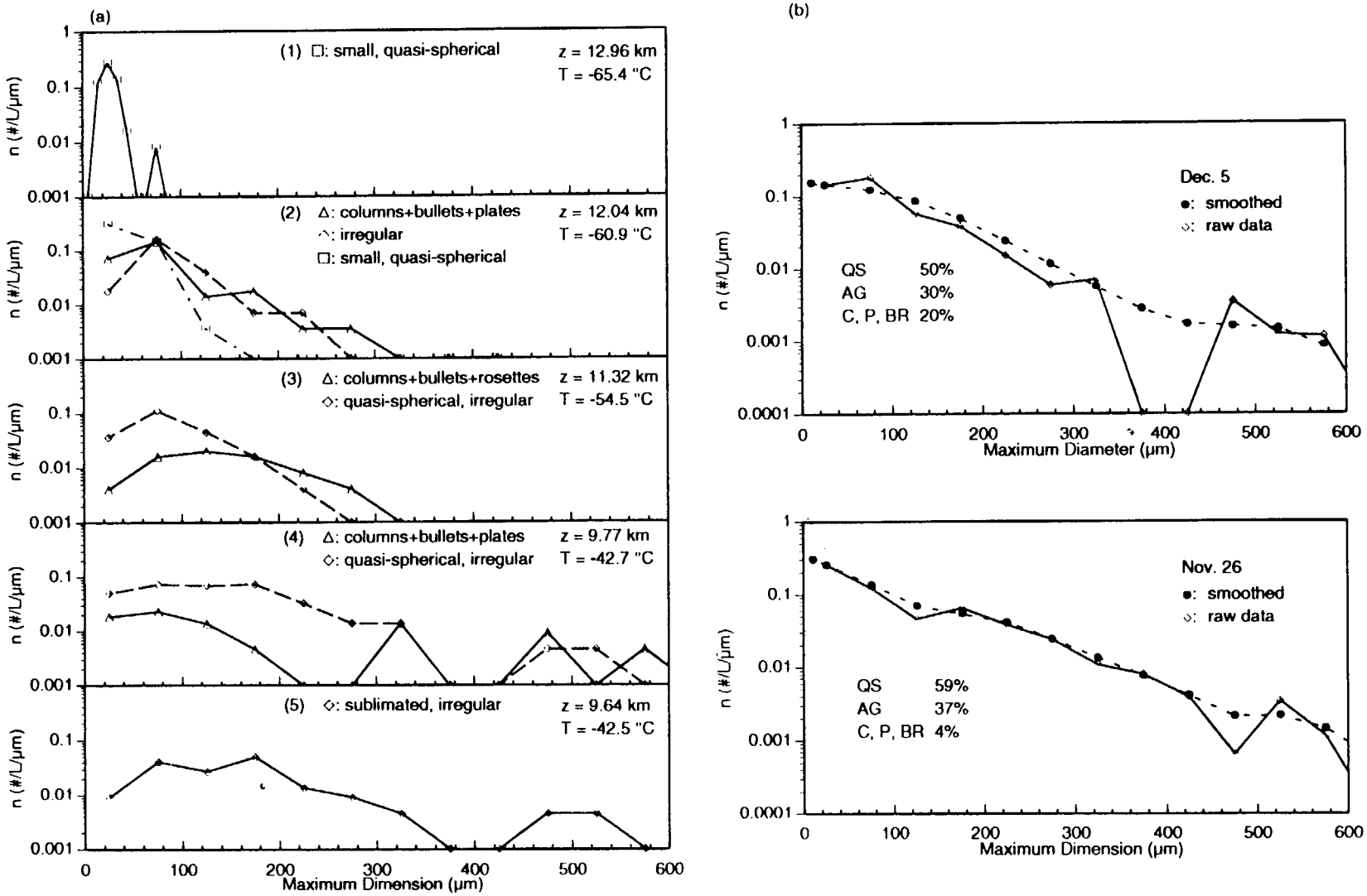

Fig. 1. (a). Five representative ice crystal size distributions derived from the replicator sounding on 5 December 1991 during FIRE-II-IFO. (b). Averaged ice crysatal size distributions and smoothed curves for 5 December and 26 November data sets. The percentages of shapes for each distribution are also shown: QS denotes quasi-spherical particles, including frozen droplets and distorted plates and columns; AG, C, P, and BR denote aggregate, column, plate and bullet rosette, respectively.

FIRE II IFO Dec.5,1991

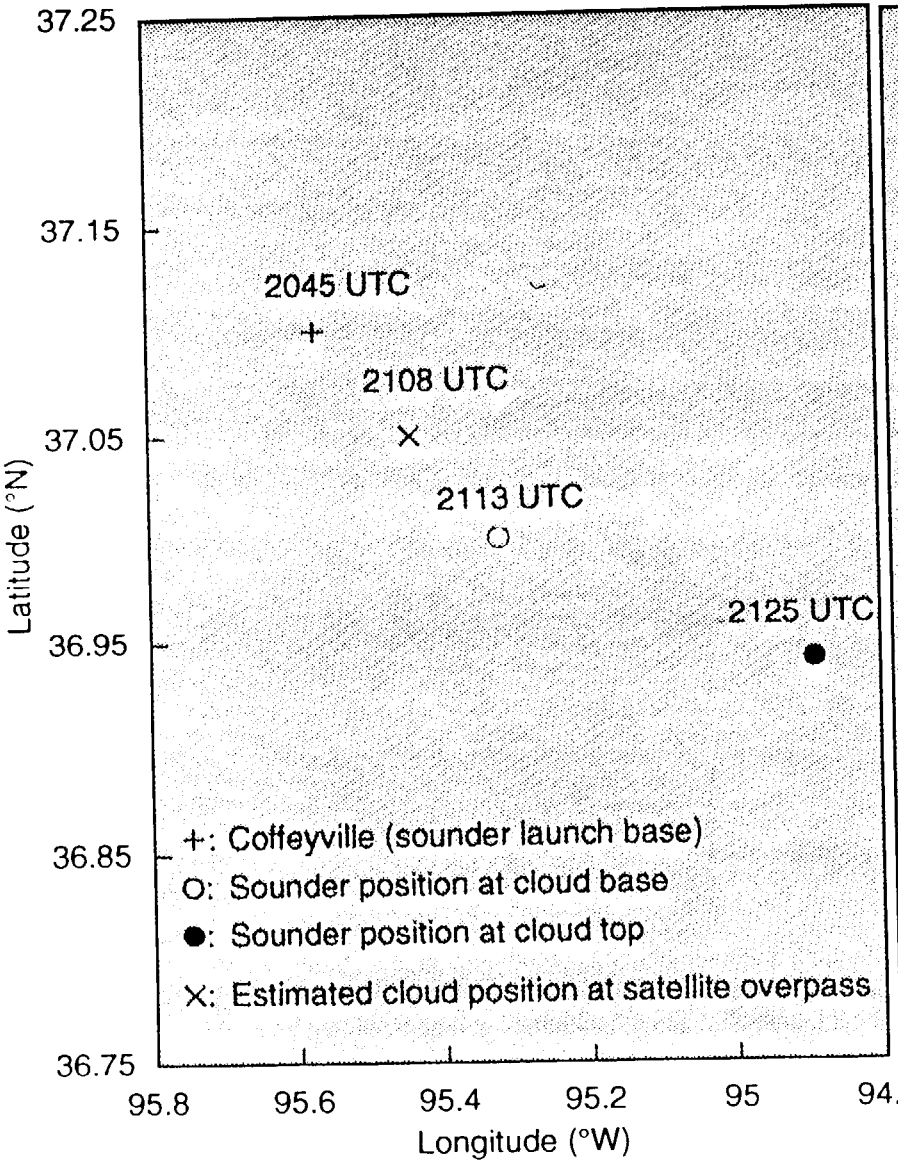

Schematic diagram of replicator sounding system

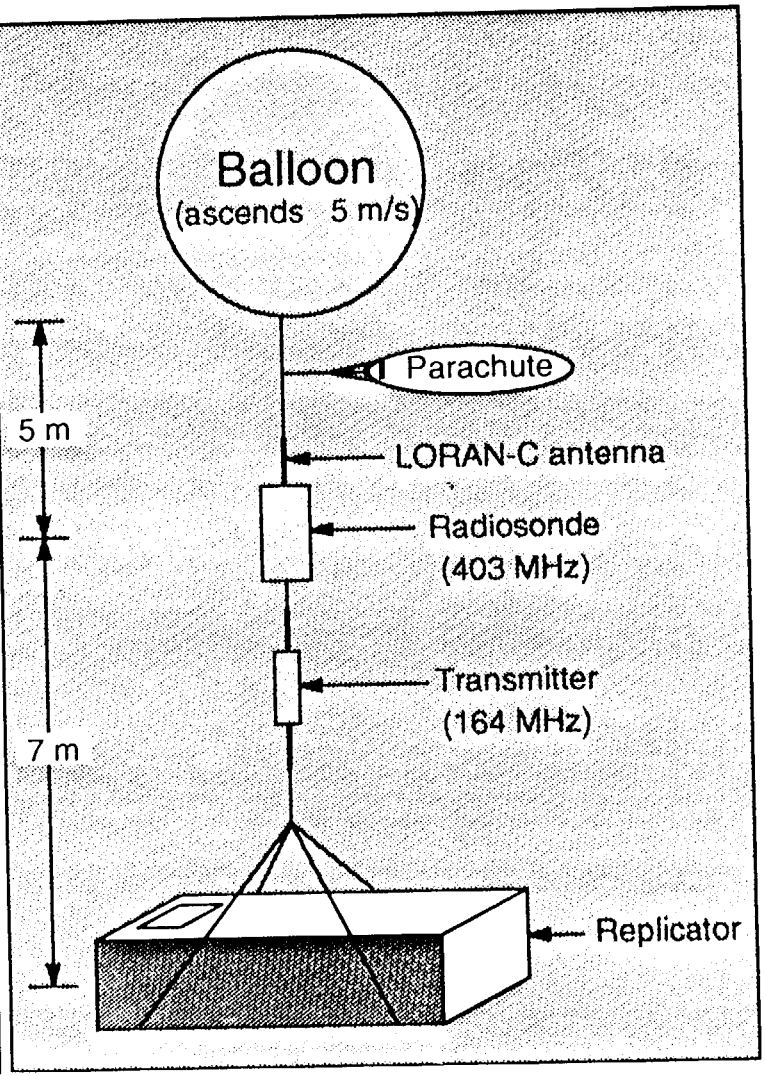

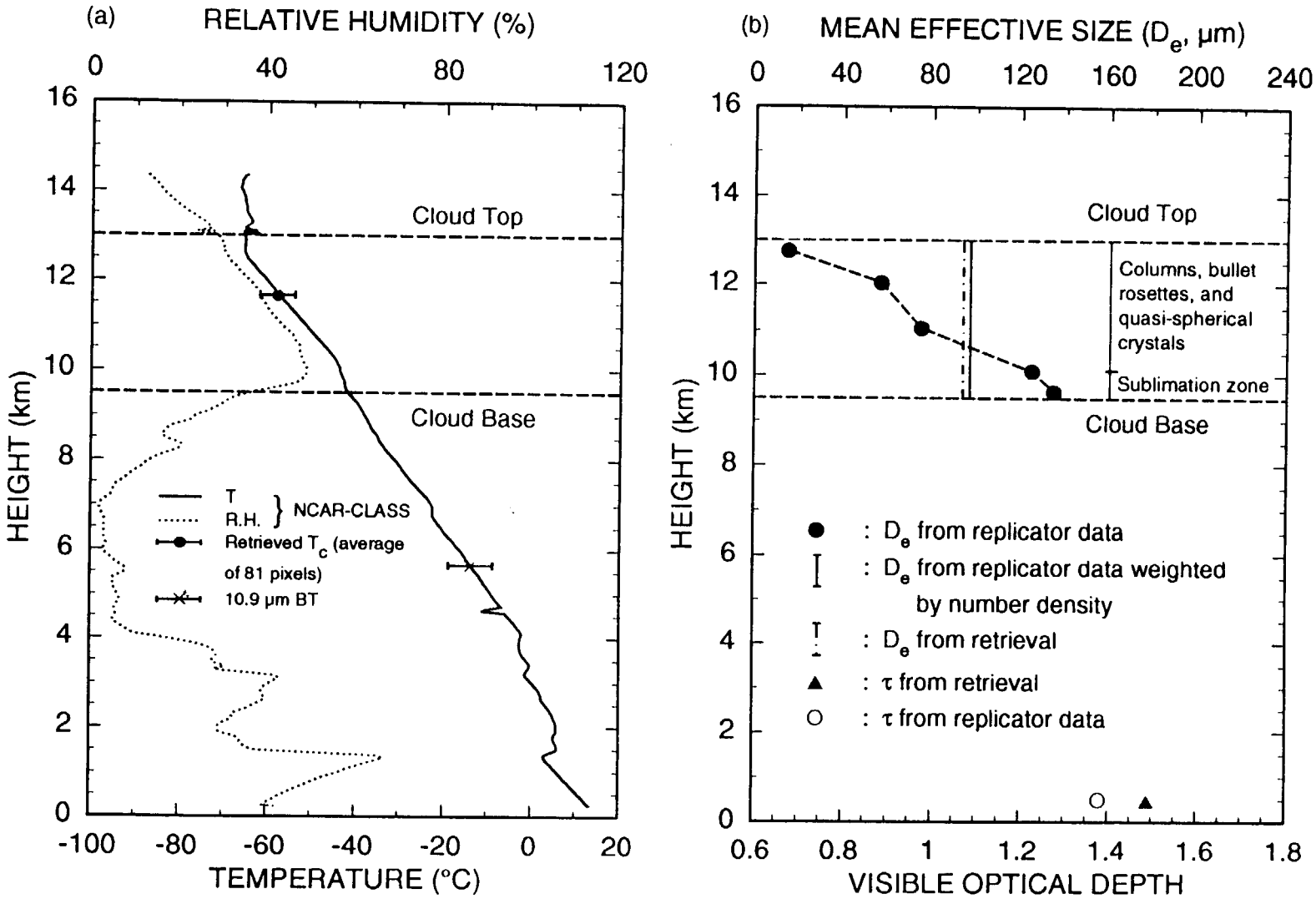

Fig. 5. (a). Temperature and humidity profiles obtained from the NCAR-CLASS sounding system on 5 December 1991. Overlapped with the temperature profile are the mean retrieved cloud temperature and mean Ch. 4 brightness temperature over a 0.05° x 0.2° domain around Coffeyville. (b). Display of the replicator-derived mean effective sizes at the selected height levels, their vertical average, and the retrieved value. Also shown on the bottom scale are the optical depths derived from the replicator data and from the retrieval.

Radiation Model

- Radiative Transfer
  Delta-four-stream (Liou, et al., 1988)
  Application to nonhomogeneous atmosphere (Liou, 1975)

- Nongray Gaseous Absorption in Scattering Atmosphere
  Correlated k-distribution approach (Fu and Liou, 1992)
  Spectral Intervals: 6 solar and 12 IR bands (Fu and Liou, 1993)

- Single-Scattering Properties of Hydrometeor
  Hexagonal ice crystal (Takano and Liou, 1989)
  Water droplet (Fu, 1991)
  Rain, Snow, and Graupel

- Vectorized Version on Supercomputer

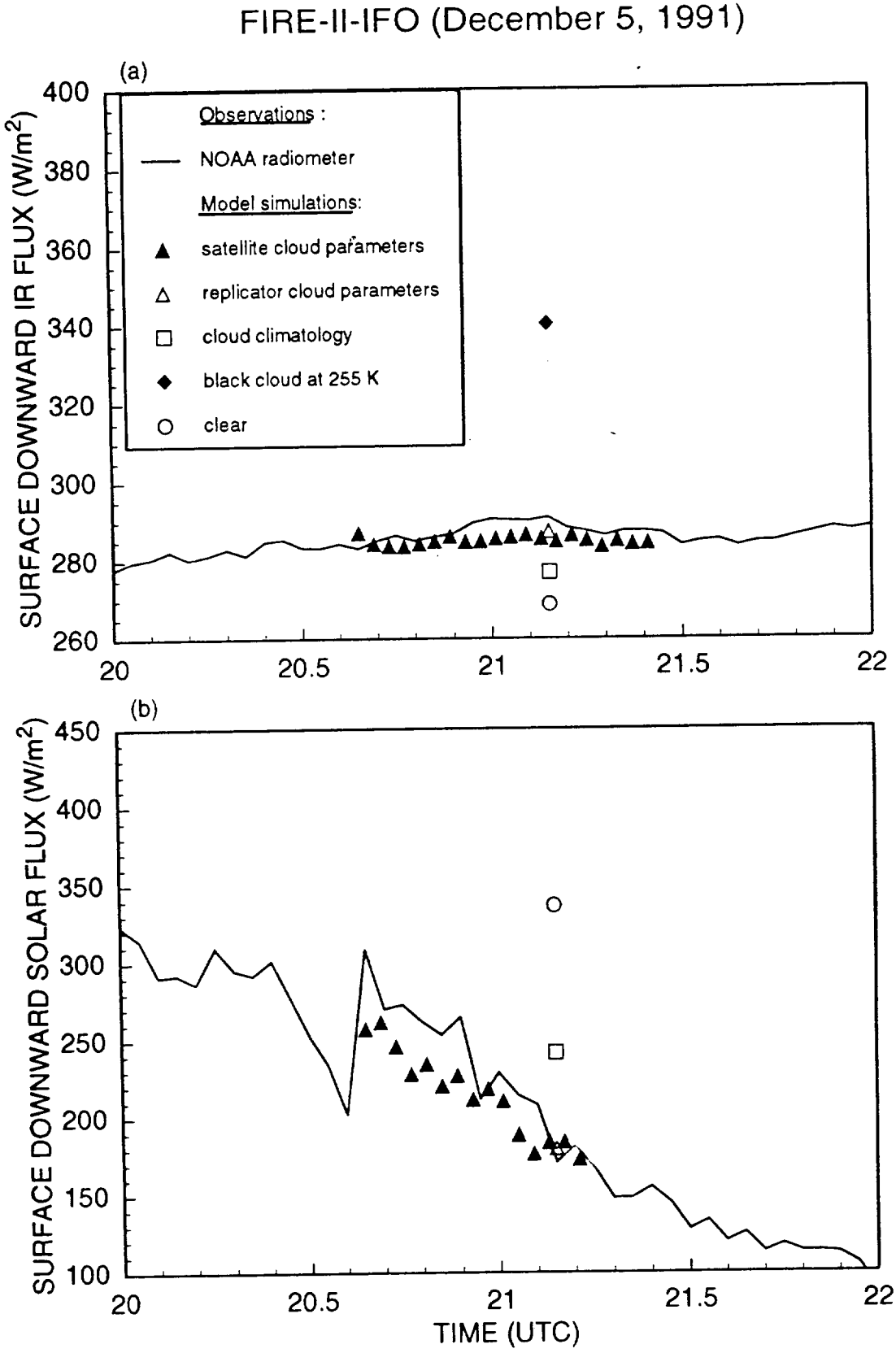
FIRE-II-IFO (December 5, 1991)
(a)
Observations :
NOAA radiometer
Model simulations:
satellite cloud parameters
replicator cloud parameters
cloud climatology
black cloud at 255 K
clear
SURFACE DOWNWARD IR FLUX (W/m2)
400
380
360
340
320
300
280
260
20
20.5
21
21.5
22
(b)
SURFACE DOWNWARD SOLAR FLUX (W/m2)
450
400
350
300
250
200
150
100
20
20.5
21
21.5
22
TIME (UTC)

FIRE-II-IFO (November 26, 1991)

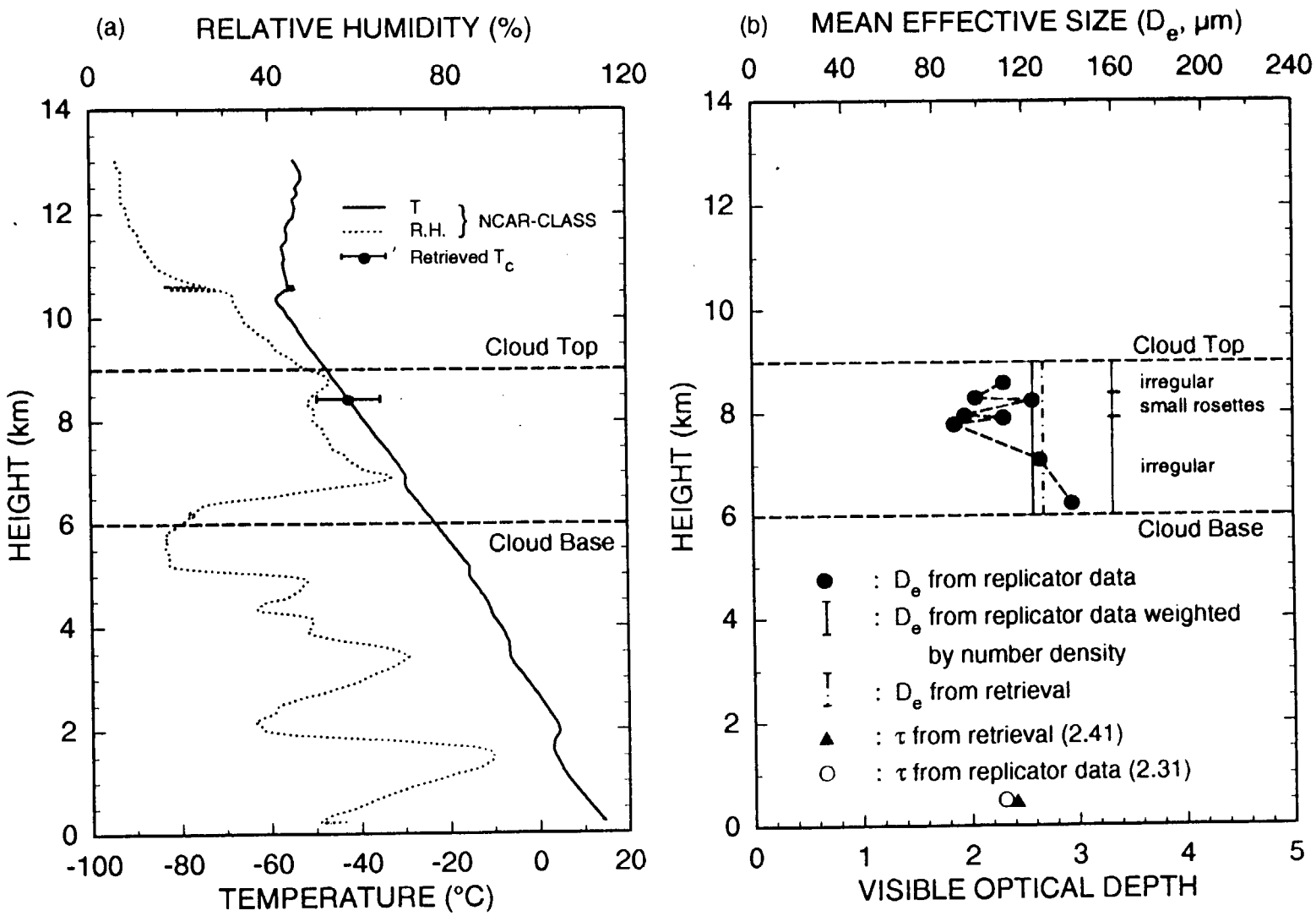

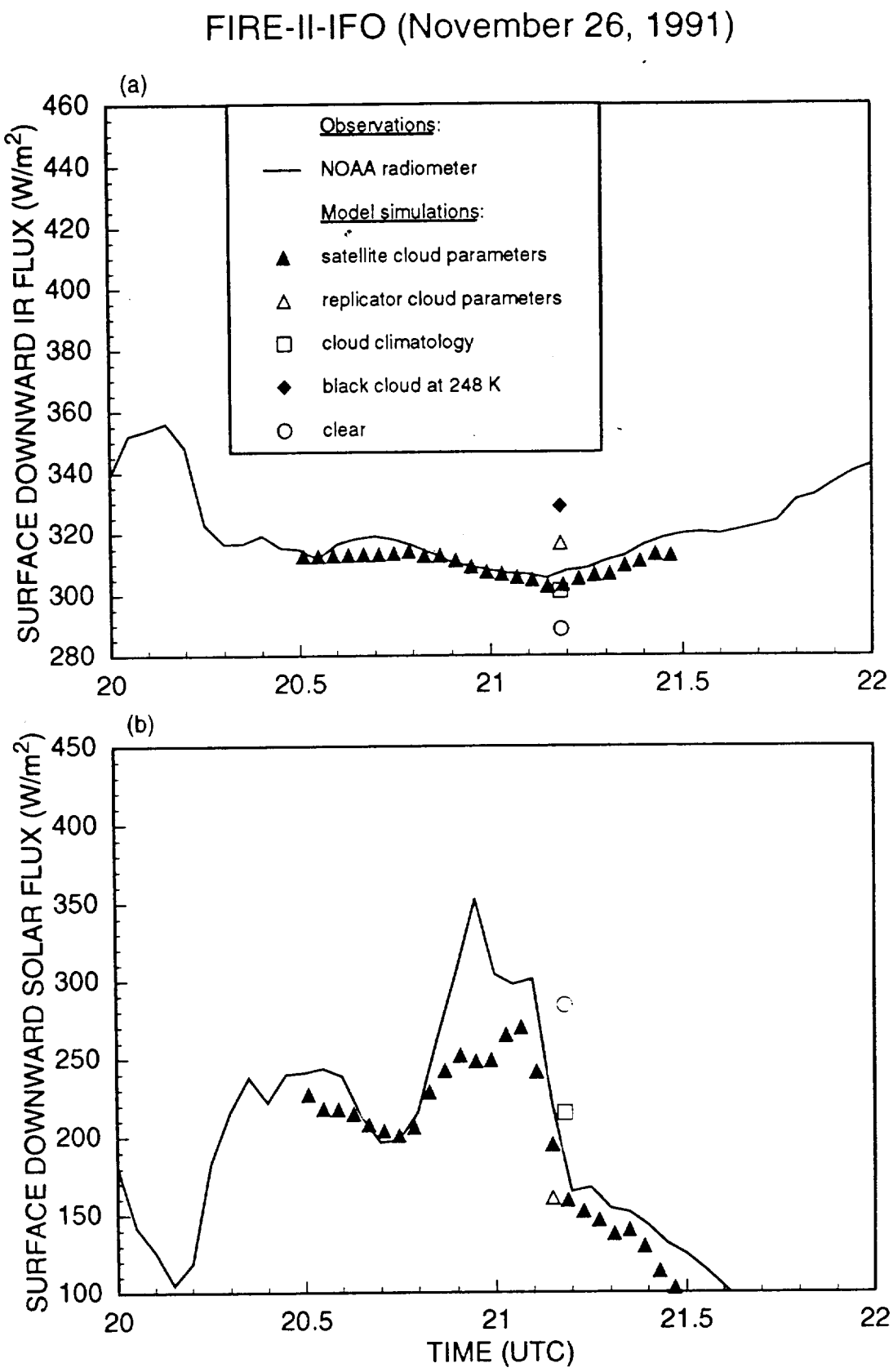
FIRE-II-IFO (November 26, 1991)
(a)
Observations:
NOAA radiometer
Model simulations:
satellite cloud parameters
replicator cloud parameters
cloud climatology
black cloud at 248 K
clear
SURFACE DOWNWARD IR FLUX (W/m2)
460
440
420
400
380
360
340
320
300
280
20
20.5
21
21.5
22
(b)
SURFACE DOWNWARD SOLAR FLUX (W/m2)
450
400
350
300
250
200
150
100
20
20.5
21
21.5
22
TIME (UTC)

Future Research

- Light Scattering by Small Ice Crystals ($10 < \alpha < 30$)
- Validation: Remote Sounding of the Cirrus Optical Depth and Ice Crystal Size in Cirrus/Low Cloud Conditions
- Development of New Techniques for the Determination of Ice Crystal Sizes Using 1.6 μm and Visible Wavelengths